Research Square

Preprints are preliminary reports that have not undergone peer review.
They should not be considered conclusive, used to inform clinical practice,
or referenced by the media as validated information.

Airborne ion charge kinetics reveal circadian-range periodicity in detached plant fruits: a continuous, noncontact, and noninvasive measurement system

Hidehiko Higaki
Kyushu Sangyo University
Hirofumi Ichiki
Kyushu Sangyo University
Toshiro Kawaguchi
kawaguchi4463@yahoo.co.jp

Kyushu Sangyo University

Research Article

Keywords: MALIC system, circadian rhythms, ion charge kinetics, airborne ions, noninvasive measurement, actogram, Lomb-Scargle periodogram, phase drift, phase coherence, apple fruit

Posted Date: May 19th, 2026

DOI: https://doi.org/10.21203/rs.3.rs-9582260/v1

License: This work is licensed under a Creative Commons Attribution 4.0 International License.
Read Full License

Additional Declarations: No competing interests reported.

Version of Record: A version of this preprint was published at Plant Methods on September 8th, 2026.
See the published version at https://doi.org/10.1186/s13007-026-01594-7.

Airborne ion charge kinetics reveal circadian-range periodicity in detached plant fruits: a continuous, noncontact, and noninvasive measurement system

Hidehiko Higaki[1], Hirofumi Ichiki[2] and Toshiro Kawaguchi[3]*

[1] Faculty of Life Science, Kyushu Sangyo University, 2-3-1, Matsukadai, Higashi-ku, Fukuoka 813-8503, Japan

[2] Faculty of Science and Engineering, Kyushu Sangyo University, 2-3-1, Matsukadai, Higashi-ku, Fukuoka 813-8503, Japan

[3] Professor emeritus, Kyushu Sangyo University, 2-3-1, Matsukadai, Higashi-ku, Fukuoka 813-8503, Japan

*Correspondence:

Toshiro Kawaguchi, PhD

Phone number +81-92-501-2816; e-mail address: kawaguchi4463@yahoo.co.jp

Abstract word count: 302; text word count: 2,561; number of figures: 7, number of references: 12

Abstract

Background Understanding temporal regulation in plant systems requires measurement approaches that capture physiological kinetics with minimal tissue perturbation. Here, we present a magnetically levitated electrode ionization chamber (MALIC) system for monitoring airborne ion charge kinetics in a continuous, noncontact, and noninvasive manner, enabling the continuous physicochemical observation of plant-derived signals without genetic modification or optical readouts.

Results Using detached fruits of two apple cultivars (Yoko and Akibae), Lomb-Scargle periodogram analysis identified dominant periodic components within the circadian range (~24–25 h) in airborne ion charge. Phase drift analysis revealed cultivar-dependent differences in temporal stability, with Yoko exhibiting relatively consistent peak timing across successive cycles, whereas Akibae showed greater variability. These differences were further supported by phase coherence analysis, which demonstrated the tighter clustering of phase values in Yoko compared with Akibae. Quantitative analysis showed that Akibae exhibited larger amplitude and a higher coefficient of variation, indicating greater relative variability. Because the MALIC system detects net ion-related signals in the surrounding air rather than intracellular processes directly, the observed oscillations should be interpreted as a proxy for integrated physiological activity. These rhythms are consistent with temporally organized physiological processes but do not establish a direct link to endogenous circadian clock mechanisms.

Conclusions The MALIC system enables the continuous, noncontact, and noninvasive measurement of airborne ion charge kinetics exhibiting reproducible circadian-range periodicity in detached plant tissues. This work establishes airborne ion charge as a previously unrecognized temporal signal at the plant–environment interface. Rather than replacing established circadian assays, the MALIC system should be considered a complementary approach that captures signals distinct from transcriptional and photosynthetic readouts. Further validation across species, cultivars, and environmental conditions, together with integrated environmental, molecular, and physiological measurements, will be essential to determine whether airborne ion charge kinetics can serve as reliable indicators of endogenous biological rhythms in plants.

Keywords MALIC system, circadian rhythms, ion charge kinetics, airborne ions, noninvasive measurement, actogram, Lomb-Scargle periodogram, phase drift, phase coherence, apple fruit

Introduction

Circadian rhythms of plants are endogenous biological oscillations with a period of approximately 24 hours that allow them to anticipate and adapt to daily environmental changes [1]. These rhythms regulate a wide range of physiological processes, including gene expression, photosynthesis, metabolism, and growth [1, 2], thereby contributing to plant fitness and productivity [1].

To date, a variety of methodologies have been developed to assess plant circadian rhythms from molecular to physiological levels [2, 3]. At the molecular level, luciferase-based reporter systems have been widely used to monitor rhythmic gene expression with high temporal resolution [4]. At the physiological level, measurements of photosynthetic activity (e.g., chlorophyll fluorescence and delayed fluorescence) have provided noninvasive approaches to capture circadian rhythms without genetic manipulation [5, 6]. Despite these advances, most existing methods rely on either genetically encoded reporters or optical signals associated with photosynthetic processes. Consequently, they primarily reflect transcriptional activity or photosynthesis-related physiology and may not fully capture alternative outputs of the circadian system. Ion transport represents a fundamental aspect of plant physiology, underpinning processes (e.g., membrane potential regulation, signal transduction, and cellular homeostasis). Emerging evidence suggests that ion transport processes are under circadian control [7, 8]. However, continuous monitoring of these kinetics in intact plant tissues remains technically

challenging, particularly under continuous, noncontact, and noninvasive conditions. In this context, ion-related physicochemical outputs represent a relatively unexplored dimension of plant circadian regulation [7, 8].

In the present study, we used the magnetically levitated electrode ionization chamber (MALIC) system [9] as a novel approach to examine plant circadian-range periodicity based on the continuous monitoring of airborne ion charge kinetics. This method does not require genetic modification and is independent of photosynthetic optical signals, thereby providing a complementary measurement modality for circadian rhythm analysis. By applying this technique under predominantly constant dark conditions with a brief light exposure, we demonstrated that ion-related signals in the air exhibited reproducible circadian-range periodicity, highlighting their potential as a noninvasive indicator of plant kinetics.

Materials and methods

MALIC system

A MALIC unit (40 cm in length; 40 cm in width; 120 cm in height) is a noncontact and noninvasive ionization chamber device that detects very low airborne ion charge (< 10 ions/mL, detection limit range) based on ionization-derived electric signals. The MALIC system used in the present study consisted of three units connected to a single computer, enabling the nonintact and real-time monitoring of airborne anion and cation charge, as well as net ion charge that was defined as the difference between anion and cation signals, expressed as ion number concentration (ions/mL) derived from charge-based measurements in the air. The measurement principles and configuration of the MALIC unit and system have been described in detail [9, 10]. A schematic diagram of the system is shown in Fig. 1.

Experimental design

Two Japanese apple cultivars (*Malus* × *domestica* 'Yoko' and 'Akibae') were used. The airborne ion charge of each cultivar was measured continuously in a separate experimental run. Fruits were placed in a transparent acrylic container (volume: 0.15 m^3; length: 50 cm; width: 50 cm; height: 60 cm; thickness: 11 mm) equipped with a light-emitting diode (LED) light for plant growth (photosynthetic photon flux density: 684 μmol/m^2/s; Alion-ots; Allion Japan, Tokyo, Japan).

In the first experiment, four Yoko fruits (mean weight: 320 g)—which had been detached approximately 6 months post-anthesis—were placed in the container within 90 minutes of detachment. The samples were exposed to the following experimental conditions: constant darkness (DD) was initiated at 15:00 on day 1 and maintained until 14:00 on day 8. This was followed by a light phase from 14:00 to 22:00 on day 8, after which the DD condition resumed until 13:00 on day 13, when the samples were removed from the container. In the second experiment, four Akibae fruits (mean weight: 330 g)—which had been detached approximately 6 months post-anthesis—were placed in the same container within 90 minutes of detachment. The samples were exposed to the following experimental conditions: DD was initiated at 15:00 on day 1 and maintained until 03:00 on day 3. This was followed by a light phase from 03:00 to 06:00 on day 3, after which the DD condition resumed until 09:00 on day 12, when the samples were removed from the container.

Under the DD condition, the container was completely covered with a black cloth (400 cm long × 200 cm wide) to ensure light exclusion. Time zero (t = 0) was defined as the onset of the initial dark phase. During the light phase, illumination was provided using the LED light. Airborne ion charge was continuously recorded at 1-h intervals throughout each experiment. Measurements were conducted under controlled environmental conditions, with temperatures ranging from 12 to 15°C and relative humidity between 40% and 60%.

Data analysis

The dataset included elapsed time (h), net ion charge (anion–cation difference), and light conditions. All analyses and figure generation were performed using Python (version 3.11–3.13; Python Software Foundation). Numerical computations and statistical analyses were conducted using NumPy and SciPy, and figures were generated using Matplotlib.

Actogram analysis

Time-series data were arranged at 1-h intervals without interpolation. Light conditions were converted to binary values (light = 1, dark = 0). Signal values were scaled to a range of 0–1 across datasets for visualization. Actograms were constructed in a 48-h double-plot format, in which each row represents consecutive 48-h windows (0–24 h and 24–48 h). Light and dark conditions were displayed as grayscale bars above each actogram.

Periodogram analysis

Periodicity was assessed using the Lomb-Scargle method implemented in the SciPy library. Time-series data were detrended by subtracting the mean value without additional filtering or smoothing. The periodogram was computed over a frequency range corresponding to periods between 5 h and 80 h. Power spectra were normalized using Lomb-Scargle normalization, and plotted against period (h). Dominant and secondary peaks were identified based on spectral power.

Statistical significance of periodicity

The statistical significance of periodic components was evaluated using an empirical false alarm probability approach based on permutation analysis. A permutation-based surrogate analysis was conducted by randomly shuffling the time-series values 1,000 times while preserving the distribution of values. For each surrogate dataset, a Lomb-Scargle periodogram was computed, and the distribution of maximum spectral power values was obtained. The maximum spectral power across all tested frequencies was extracted for each surrogate dataset to account for multiple testing. The 95th percentile of this distribution was used as the empirical significance threshold ($p < 0.05$).

Phase drift and coherence analysis

Phase drift analysis was conducted to evaluate temporal changes in the peak timing of net ion charge. For each consecutive 24-h window starting at $t = 0$, the phase was defined as the time point at which the net ion charge difference reached its maximum value. When multiple time points exhibited the same maximum value within a window, their mean time was used. All 24-h windows were included in the analysis, including incomplete windows at the end of the time series.

Phase values were converted to angular values (θ) using the transformation $\theta = 2\pi \times \text{phase} / 24$ and represented on a circular scale. Phase coherence was quantified using the mean resultant vector. The length of the mean result vector (R) value was used as an index of phase clustering, where values close to 1 indicate strong coherence and values close to 0 indicate dispersion.

Variability analysis

The coefficient of variation (CV) was calculated as the standard deviation divided by the mean.

Results

System configuration and analytical workflow

A schematic overview of the MALIC system is shown in Fig. 1. The system enables the continuous airflow-based measurement of airborne cation and anion charge, from which net ion charge was calculated at 1-h intervals. The total airflow rate was maintained at 6 L/min and equally distributed across individual MALIC units.

The analytical workflow applied to the time-series data is illustrated in Fig. 2. Time-series ion charge data illustrated in Fig. 3 were first visualized using actograms to assess rhythmic patterns, followed by periodicity analysis using Lomb-Scargle periodograms with empirical significance thresholds. The temporal stability of detected rhythms was further evaluated using phase drift and phase coherence analyses.

Airborne ion charge kinetics

Time-course analysis revealed clear differences in ion charge kinetics between the two cultivars (Fig. 3), with ion charge (coulomb) converted to ion charge (ion/mL). Yoko (Fig. 3A) exhibited relatively stable oscillatory behavior with moderate fluctuations throughout the measurement period. In contrast, Akibae (Fig. 3B) showed large-amplitude fluctuations and transient high-intensity peaks following light exposure, resulting in greater temporal variability. The duration of measurement differed between cultivars according to the experimental design.

Quantitative analysis confirmed these differences (Fig. 3C, D). The mean net ion charge was substantially lower in Yoko (mean ± SD: 2.87 ± 1.15 ions/mL) than in Akibae (mean ± SD: 7.76 ± 9.09 ions/mL). CV was also lower in Yoko (0.40) than in Akibae (1.17). In Yoko, net ion charge exhibited relatively stable oscillatory behavior with moderate fluctuations.

Circadian patterns visualized by actograms

Actogram analysis revealed distinct rhythmic patterns in net ion charge for both cultivars (Fig. 4). Yoko (Fig. 4A) exhibited relatively stable and consistent daily oscillations with regular timing and intensity across successive days. In contrast, Akibae (Fig. 4B) showed greater variability in both signal intensity and temporal pattern, indicating reduced regularity of rhythmic behavior.

Periodicity of ion charge kinetics

To assess whether the observed temporal patterns reflected underlying periodicity, Lomb-Scargle periodogram analysis was conducted (Fig. 5). Both Yoko (Fig. 5A) and Akibae (Fig. 5B) exhibited dominant periodic components within the circadian range (~24–25 h). Akibae additionally displayed secondary peaks outside the circadian range, suggesting the presence of more complex or less synchronized oscillatory components.

Phase stability of rhythmic oscillations

Phase drift analysis revealed clear differences in temporal stability between the two cultivars

(Fig. 6). In Yoko (Fig. 6A), the timing of peak ion charge remained relatively consistent across consecutive days, indicating stable phase positioning. In contrast, Akibae (Fig. 6B) exhibited greater variability in peak timing, with noticeable day-to-day fluctuations.

Phase coherence differs between cultivars

Circular representations of phase values revealed distinct differences in phase coherence between cultivars (Fig. 7). In Yoko (Fig. 7A), phase values were tightly clustered within a narrow angular range, indicating the consistent timing of peak net ion charge difference across successive 24-h windows. In contrast, Akibae (Fig. 7B) exhibited a broader distribution of phase values, suggesting greater variability in peak timing. Consistent with these observations, the R value was higher in Yoko ($R = 0.84$, $n = 12$) than in Akibae ($R = 0.59$, $n = 11$), indicating stronger phase coherence in Yoko.

Summary of temporal characteristics

Taken together, both cultivars exhibited significant circadian-range periodicity in airborne ion charge kinetics. However, the temporal structure of these oscillations differed markedly between cultivars. Yoko showed relatively stable and coherent rhythmicity, whereas Akibae exhibited larger amplitude fluctuations, additional periodic components, and reduced phase stability. These results indicate that cultivar-dependent differences exist not only in the magnitude of ion charge fluctuations but also in the stability and organization of their kinetics.

Discussion

The MALIC system enables continuous, noncontact, noninvasive, and nongenetic measurement of airborne ion charge, providing a physicochemical modality distinct from conventional circadian assays based on transcriptional reporters or photosynthesis-related optical signals [5, 6]. Because the system detects net ion charge in the surrounding air rather than intracellular ion fluxes or gene expression, it should be interpreted as an integrated proxy of physiological activity at the tissue or organ level. This framework extends applicability to non-model species and postharvest materials while allowing long-term monitoring without tissue perturbation.

Time-course analysis showed that net ion charge closely tracked anion signals, indicating that overall dynamics were predominantly driven by anion contributions. Despite transient perturbation during the light phase, Yoko rapidly recovered its oscillatory pattern, suggesting a stable underlying temporal structure. In contrast, Akibae displayed pronounced stimulus-associated responses, with coordinated high-intensity peaks in both anion and cation charge following light exposure. These responses produced large fluctuations in net ion charge followed by rapid attenuation, indicating a transition from an activated to a more stabilized state. Taken together, these findings demonstrate that airborne ion charge captures structured temporal dynamics in plant tissues, revealing cultivar-dependent organization of physiological activity.

Actogram and spectral analyses further supported the presence of reproducible circadian-range periodicity (~24–25 h) in detached fruits. While precise period estimates depend on

analytical parameters, the consistent detection of circadian-range components indicates sustained temporal organization after harvest. However, because the MALIC system does not directly measure canonical circadian outputs, these oscillations should be interpreted as circadian-consistent rather than as direct evidence of endogenous clock activity.

Phase analysis revealed clear differences in temporal stability between cultivars. Yoko exhibited tightly clustered peak timing and high phase coherence ($R = 0.84$), whereas Akibae showed broader phase dispersion and lower coherence ($R = 0.59$), indicating reduced temporal precision. Notably, phase coherence was dissociable from oscillation amplitude, suggesting that rhythmic strength and temporal stability represent distinct properties of ion charge kinetics. These differences may reflect variation in physiological regulation, potentially involving stomatal activity, transpiration-driven ion transport, and electrochemical interactions at the tissue–air interface. These results demonstrate that airborne ion charge constitutes a structured temporal signal in plant systems.

In this context, the MALIC system provides a distinct observational layer that complements established circadian approaches. Whereas transcriptional and photosynthetic assays target specific molecular or physiological outputs [1, 5, 6], airborne ion charge signals likely integrate multiple processes, including ion transport, water flux, and surface electrochemical dynamics. This integrative nature enables the detection of emergent temporal patterns not accessible through conventional single-pathway measurements.

The observed oscillatory behavior is broadly consistent with previous studies demonstrating the circadian regulation of ion transport, membrane potential dynamics, and metabolic processes

in plants [7, 8, 11, 12]. These findings support the plausibility that ion-related physiological processes contribute to temporally structured outputs. However, the present data do not establish a mechanistic link between airborne ion charge kinetics and intracellular circadian oscillators. Direct validation using molecular and physiological markers will therefore be required to determine the extent to which these signals reflect endogenous circadian regulation.

A gradual decline in oscillation amplitude during later stages suggests progressive physiological changes associated with postharvest status. This observation raises the possibility that airborne ion charge kinetics may serve as an early indicator of physiological transitions, although this interpretation remains preliminary and requires further validation.

Several limitations should be noted. First, measurements represent aggregate signals from multiple fruits, precluding the assessment of individual variability and synchronization. Second, the mechanisms underlying airborne ion emission also remain unresolved. Addressing these limitations through integrated environmental monitoring and molecular validation will be essential for establishing the biological origin and significance of these signals.

Conclusions

The MALIC system enables continuous, noncontact, and noninvasive measurement of airborne ion charge exhibiting reproducible circadian-range periodicity in detached plant tissues. These results indicate that ion-based measurements provide a novel physicochemical perspective on

temporal physiological dynamics in plants. This work establishes airborne ion charge as a previously unrecognized temporal signal at the plant–environment interface. Rather than replacing established circadian assays, the MALIC system should be considered a complementary approach that captures signals distinct from transcriptional and photosynthetic readouts. Further validation across species, cultivars, and environmental conditions, together with integrated environmental, molecular, and physiological measurements, will be essential to determine whether airborne ion signals can serve as reliable indicators of endogenous biological rhythms in plants.

Acknowledgments

The authors are grateful to Satoshi Sakima, MD, for in-depth discussions about the manuscript.

Author contributions

T.K. designed the study; T.K., H.H., and H.I. conducted the experiments and collected images; T.K. wrote the first draft; all authors reviewed the manuscript.

Funding

The authors have not received funding for this study.

Data availability

Data are available upon a reasonable request to the corresponding author.

Declarations

Ethics approval and consent to participate

Not applicable.

Consent for publication

Not applicable.

Competing interests

The authors declare no competing interests.

References

1. Dodd AN, Belbin FE, Frank A, Webb AAR. Interactions between circadian clocks and photosynthesis for the temporal and spatial coordination of metabolism. Frontiers in Plant Science 2015, Volume 6 - 2015. https://www.frontiersin.org/journals/plant-science/articles/10.3389/fpls.2015.00245.
2. Millar AJ. The intracellular dynamics of circadian clocks reach for the light of ecology and evolution. Annu Rev Plant Biol 2016, 67:595–618. https://www.ncbi.nlm.nih.gov/pubmed/26653934.
3. McClung CR. Plant circadian rhythms. Plant Cell 2006, 18:792–803. https://www.ncbi.nlm.nih.gov/pubmed/16595397.
4. Millar AJ, Carre IA, Strayer CA, Chua NH, Kay SA. Circadian clock mutants in Arabidopsis identified by luciferase imaging. Science 1995, 267:1161–1163. https://www.ncbi.nlm.nih.gov/pubmed/7855595.
5. Gould PD, Diaz P, Hogben C, Kusakina J, Salem R, Hartwell J, Hall A. Delayed fluorescence as a universal tool for the measurement of circadian rhythms in higher plants. Plant J 2009, 58:893–901. https://www.ncbi.nlm.nih.gov/pubmed/19638147.
6. Murchie EH, Lawson T. Chlorophyll fluorescence analysis: a guide to good practice and understanding some new applications. J Exp Bot 2013, 64:3983–3998. https://www.ncbi.nlm.nih.gov/pubmed/23913954.
7. Haydon MJ, Bell LJ, Webb AA. Interactions between plant circadian clocks and solute transport. J Exp Bot 2011, 62:2333–2348.

8. Haydon MJ, Román Á, Arshad W. Nutrient homeostasis within the plant circadian network. Frontiers in Plant Science 2015, Volume 6 - 2015. https://www.frontiersin.org/journals/plant-science/articles/10.3389/fpls.2015.00299.
9. Kawaguchi T, Mukae K, Takahashi Y, Ichiki H. A novel measuring system enables the noncontact real-time monitoring of very low net concentrations of plant-emitted ions in the air that may serve for plant ion homeostasis research. BMC Plant Biol 2025, 25:1007. https://www.ncbi.nlm.nih.gov/pubmed/40751136.
10. Kawaguchi T, Futagami K, Matoba M, Wakabayashi G, Ikeda N, Uozumi Y, Yamanaka N, Kaneko M. Low-level radiation measuring system using magentically leviated electrode lonization chamber. IEEE Trans Nuc Sci 2006, 53:2276-–2280.
11. Damineli DSC, Portes MT, Feijó JA. Electrifying rhythms in plant cells. Curr Opin Cell Biol 2022, 77:102113. https://www.sciencedirect.com/science/article/abs/pii/S0955067422000667?via%3Dihub.
12. Blatt MR. A charged existence: A century of transmembrane ion transport in plants. Plant Physiol 2024, 195:79–110. https://www.ncbi.nlm.nih.gov/pubmed/38163639.

Figure legends

Fig. 1 Schematic representation of the MALIC system for monitoring airborne ion charge kinetics

The MALIC system consists of three interconnected ionization chamber units enabling the continuous, noninvasive measurement of airborne anion and cation charge, from which net ion charge (anion–cation charge difference) is derived. The system detects low-level ion charge (< 10 ions/mL) based on ionization-derived electrical signals. Orange, green, and blue lines indicate unfiltered ambient air, filtered ambient air, and ion-free filtered air (anion-free or cation-free), respectively.

LED, light-emitting diode; MALIC, magnetically levitated electrode ionization chamber

Fig. 2 Workflow for the time-series analysis of airborne ion charge kinetics

Analytical workflow applied to the time-series data of net ion charge, including the visualization of rhythmic patterns using actograms, the detection of periodicity using Lomb-Scargle periodograms, and the evaluation of temporal stability using phase drift and phase coherence analyses.

Fig. 3 Time-course changes and quantitative analysis of airborne ion charge kinetics measured by the MALIC system

Net ion charge was defined as the difference between anion and cation signals, expressed as ion number concentration (ions/mL) derived from charge-based measurements in the air (**A, B**). The

time-series profiles of airborne ion charge kinetics in Yoko (**A**) and Akibae (**B**), showing anion, cation, and net ion charge. The left and right ends of the x-axis indicate the time of fruit placement and removal, respectively. Time zero (t = 0) corresponds to the onset of the initial dark phase. Shaded regions indicate light phases. (**C**) Mean net ion charge calculated across the entire measurement period. Bars represent mean values and error bars indicate standard deviation. (**D**) Coefficient of variation was calculated from the entire time-series data for each cultivar.

Fig. 4 Actograms of airborne ion charge kinetics in apple cultivars

Actograms were constructed from the time-series data of net ion charge arranged at 1-h intervals without interpolation to preserve the original temporal structure. Signal values were normalized to a range of 0–1 for visualization. Each row represents a 48-h double plot (0–24 h and 24–48 h) to facilitate the visualization of rhythmic patterns. Light and dark conditions are indicated by grayscale bars above each actogram (white, light; black, dark).

(A) Yoko; (B) Akibae

Fig. 5 Detrended Lomb-Scargle periodograms of ion charge kinetics in apple cultivars

The time-series data of net ion charge were detrended by mean-centering and analyzed using the Lomb-Scargle method. Normalized spectral power is plotted against period (h). The dashed horizontal line indicates the empirical significance threshold ($p < 0.05$) determined using

permutation-based surrogate analysis (1,000 iterations), and the vertical dashed line indicates the dominant period.

(A) Yoko; (B) Akibae

Fig. 6 Phase drift analysis of circadian-range oscillations of airborne ion charge kinetics in apple cultivars

Phase drift analysis was conducted to evaluate the temporal stability of peak timing across consecutive circadian cycles. For each 24-h window starting at t = 0, phase was defined as the time point at which net ion charge reached its maximum value. All windows, including incomplete windows at the end of the time series, were included.

(A) Yoko; (B) Akibae

Fig. 7 Circular analysis of the phase of maximum net ion charge difference across consecutive 24-h windows

Phase values corresponding to the time of maximum net ion charge difference (anion–cation) within each 24-h window were converted to angular values ($\theta = 2\pi \times \text{phase} / 24$) and plotted on a circular scale. Each point represents one 24-h window.

The mean resultant vector was calculated to quantify phase coherence using circular statistics. The direction of the vector indicates the mean phase, and its length (mean resultant length, R)

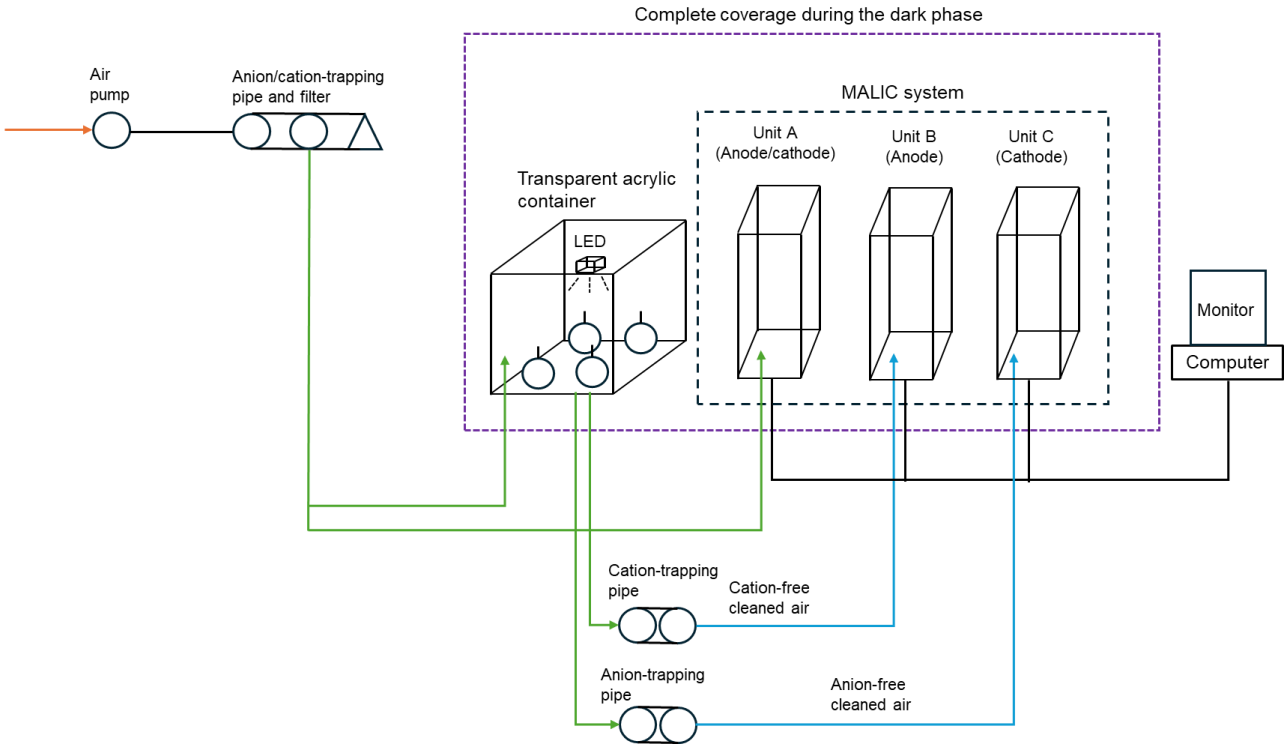
reflects the degree of phase clustering, where values close to 1 indicate strong phase coherence and values close to 0 indicate phase dispersion.

Blue points indicate the phase values for individual windows, and arrows represent the mean resultant vectors.

(A) Yoko dataset showing strong phase coherence (R = 0.84, n = 12).

(B) Akibae dataset showing moderate phase coherence (R = 0.59, n = 11).

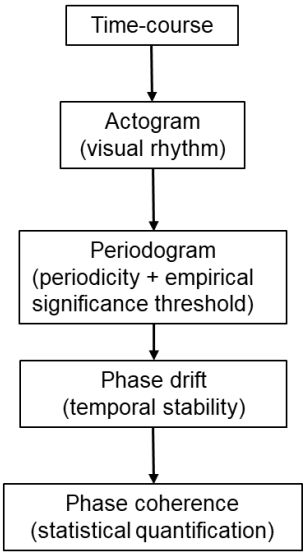
Figure 1



421

422

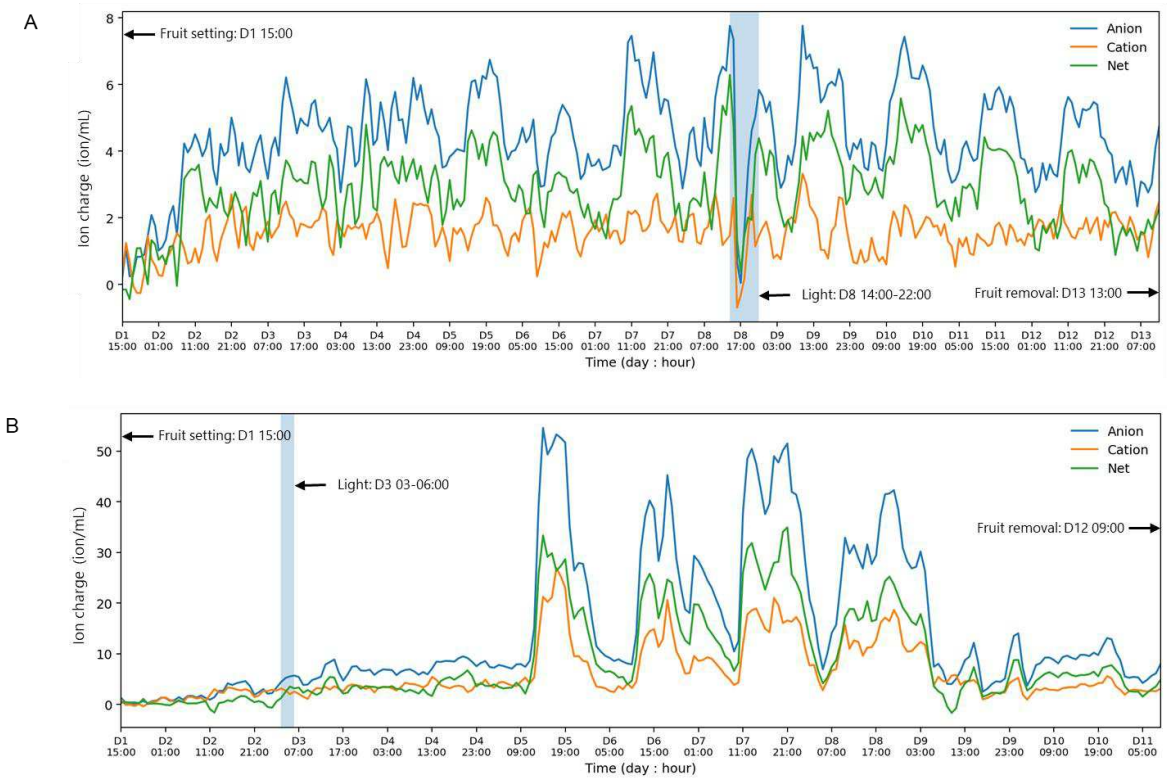
Figure 2



423

424

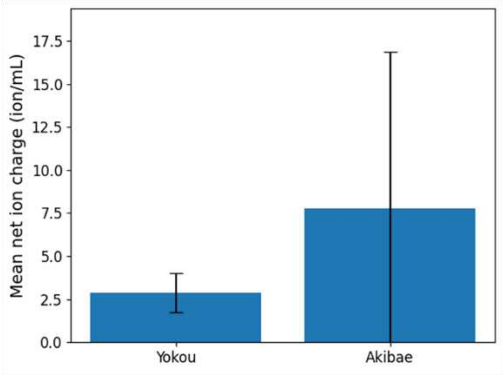
Figure 3



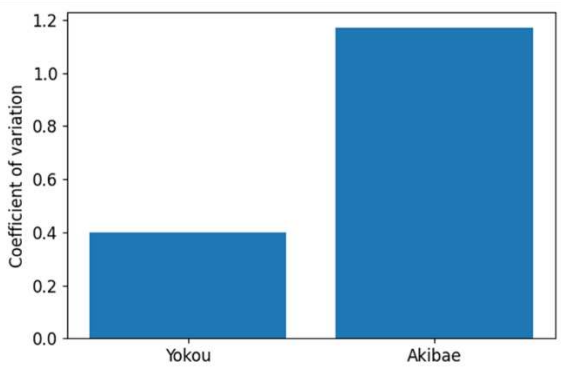
425
426

Figure 3

C



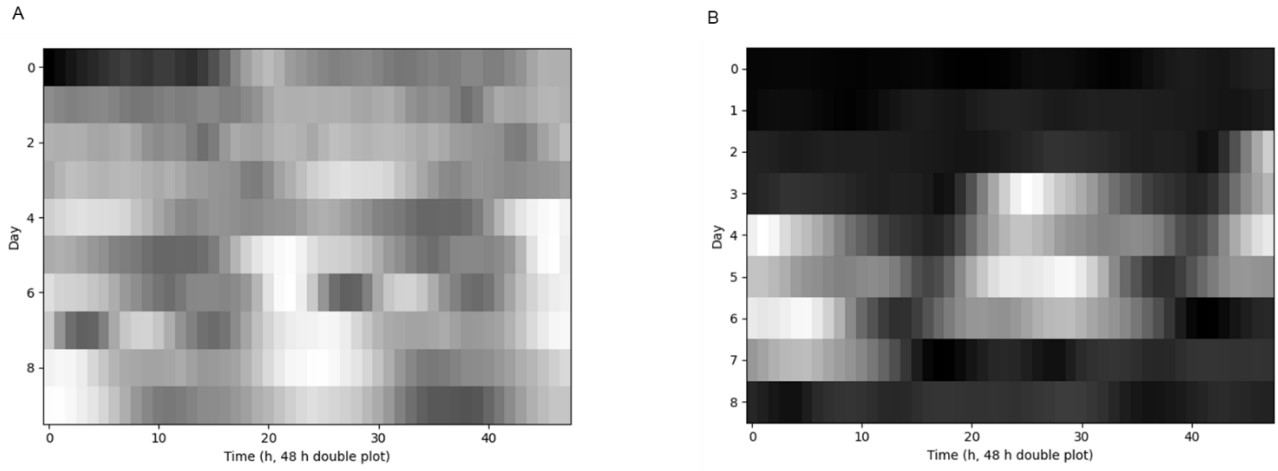
D



427

428

Figure 4

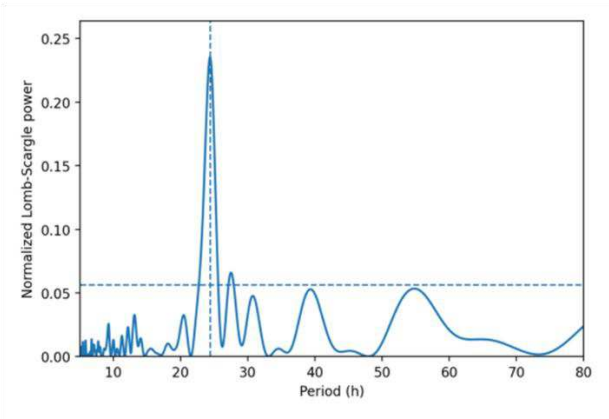


429

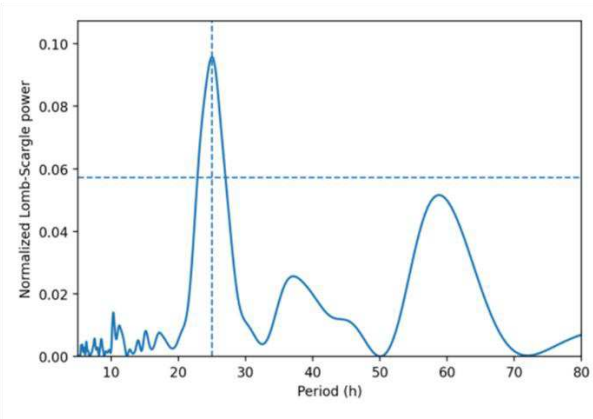
430

Figure 5

A

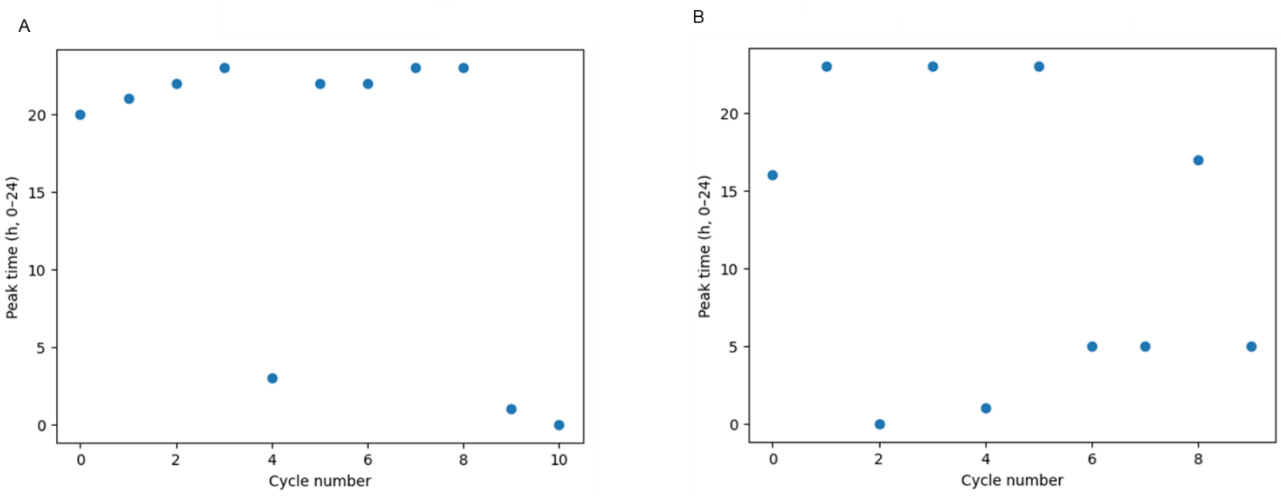


B



431

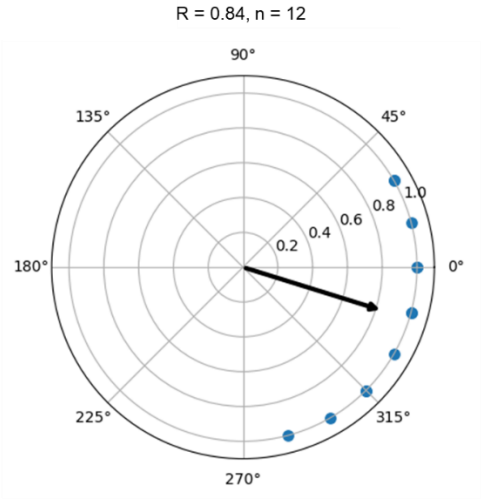
Figure 6



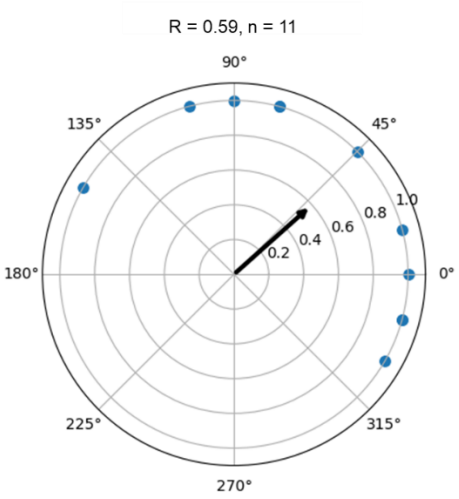
432

Figure 7

A



B



433